Supporting Information for

The 2020 Mw 6.6 Vernadsky transform earthquake sequence: rupture and Coulomb stress changes surrounding an oceanic core complex

Guilherme W. S. de Melo [1], Neil C. Mitchell[2], Sergey Y. Sokolov[3]

[1] GEOMAR Helmholtz Centre for Ocean Research Kiel, Kiel, Germany

[2] Department of Earth and Environmental Sciences, University of Manchester, Manchester, United Kingdom

[3] Geological Institute, Russian Academy of Sciences, Moscow, Russia

This document provides supporting material for the manuscript(23 figures and three tables). Crustal age constraints along the Vernadsky transform fault obtained from global data set of Seton et al. (2020) is shown in Fig.S1. Fig.S2-S13 shows the 24-hour helicorder plots of the NBMO station located in NE Brazil with the record of the seismicity filtered with a Butterworth 3-6 Hz bandpass. Results of relative relocation (McGuire., 2008) of four earthquakes with Mw>4.9 using data from 34 stations are showed in Fig.S14-S17. The ISOLA (Zahradník and Sokos., 2018) best-fitting waveform model for the Mw 5.8 aftershock is presented in Fig.S18. Fig.S19 shows the 2D grid of the rupture parameters for the Coulomb3 (Toda et al., 2011) model of static stress change. Fig.S20 shows the Coulomb stress change model generated only by the Mw 6.6 using Coulomb3, assuming the vertical faulting range was 8, 10, and 12 km. Fig.S21 shows similar modeling results of static Coulomb stress obtained using DIS3D (Fialko and Rubin., 1999). Table S01 (additional file) contains the velocity model used in the study and based on CRUST 1.0 (Laske et al., 2013). Table S02 (additional file) is the complete catalog of earthquakes located in our study using HYPO71 (Lee and Valdes., 1985). Table S3 (additional file) contains the new epicentral coordinates of those events after relocating with HYPODD.

References

Fialko, Y. A., and Rubin, A. M. (1999). What controls the along-strike slopes of volcanic rift zones?. Journal of Geophysical Research: Solid Earth, 104(B9), 20007-20020.

Laske, G., Masters, G., Ma, Z., and Pasyanos, M. (2013, April). Update on CRUST1. 0—A 1-degree global model of Earth's crust. In Geophysical research abstracts (Vol. 15, No. 15, p. 2658). Vienna, Austria: EGU General Assembly.

Lee, W. H. K., and Valdes, C. M. (1985). HYPO71PC: A personal computer version of the HYPO71 earthquake location program (Vol. 85, No. 749). US Geological Survey.

McGuire, J. J. (2008). Seismic cycles and earthquake predictability on East Pacific Rise transform faults. Bulletin of the Seismological Society of America, 98(3), 1067-1084.

Seton, M., Müller, R. D., Zahirovic, S., Williams, S., Wright, N. M., Cannon, J., ... McGirr, R. (2020). A global data set of present-day oceanic crustal age and seafloor spreading parameters. Geochemistry, Geophysics, Geosystems, 21(10), e2020GC009214.

Toda, S., Stein, R. S., Sevilgen, V., and Lin, J. (2011). Coulomb 3.3 Graphic-rich deformation and stress-change software for earthquake, tectonic, and volcano research and teaching—user guide. US Geological Survey open-file report, 1060(2011), 63.

Zahradník, J., and Sokos, E. (2018). ISOLA code for multiple-point source modeling. In Moment Tensor Solutions (pp. 1-28). Springer, Cham.

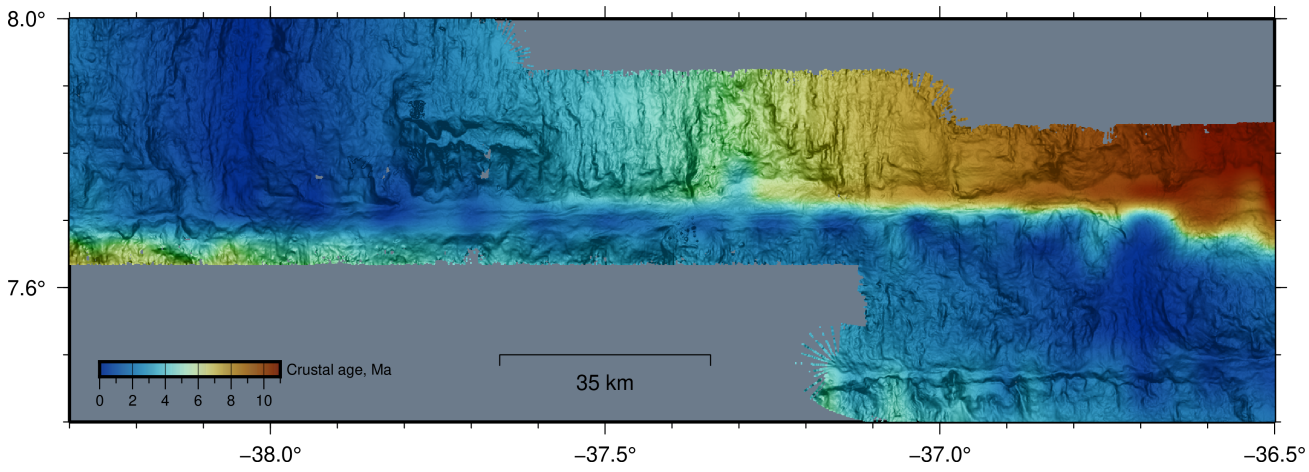

Figure 1: Shaded multibeam bathymetry of the Vernadsky transform, equatorial Atlantic. The map color shows the crustal age variation along the transform fault (Seton et al. 2020).

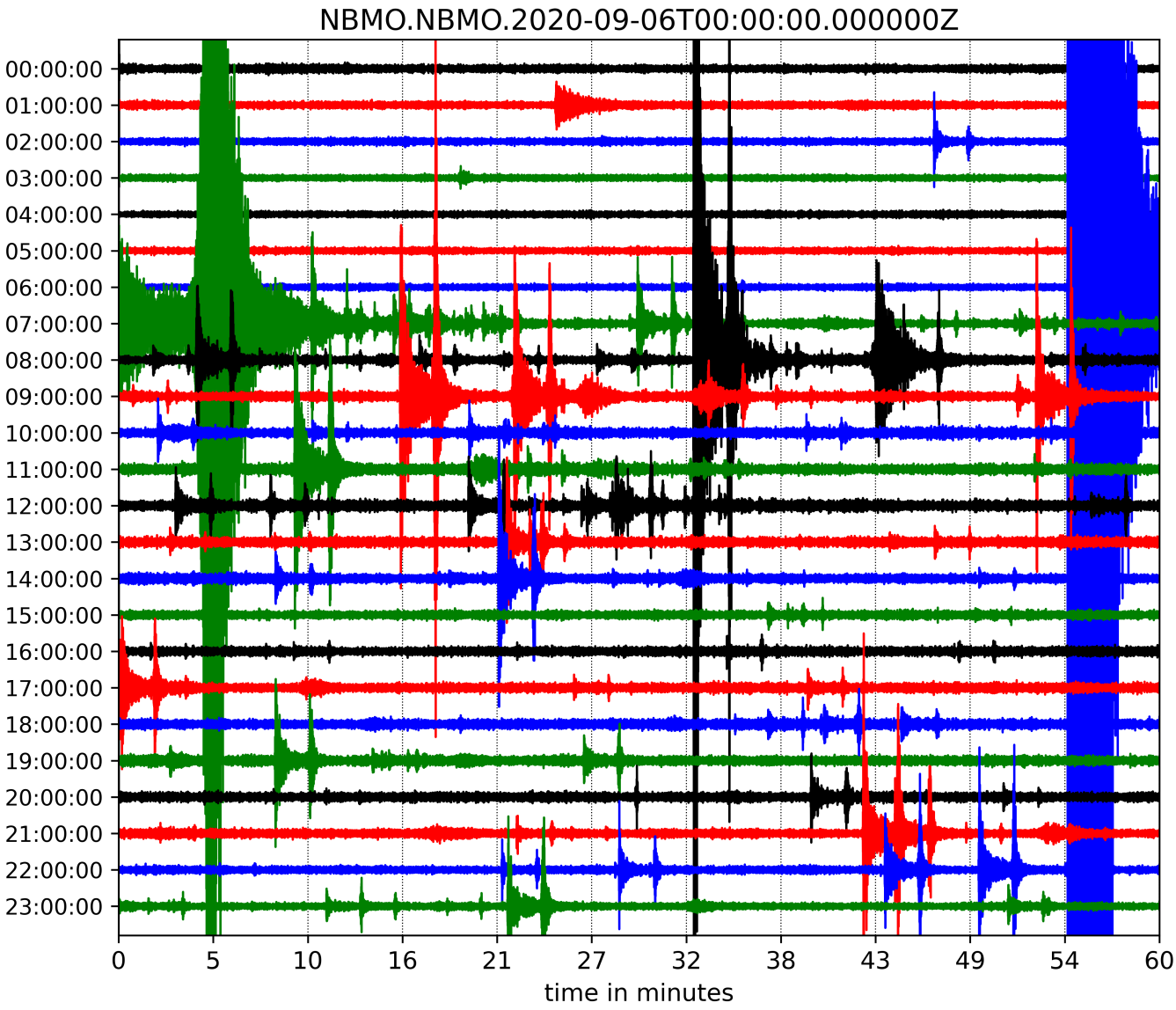

Figure 2: The 24 hour helicorder plot from the vertical component of NBMO seismic station for September 6, 2006. Horizontal colored lines present hour by hour interval time.

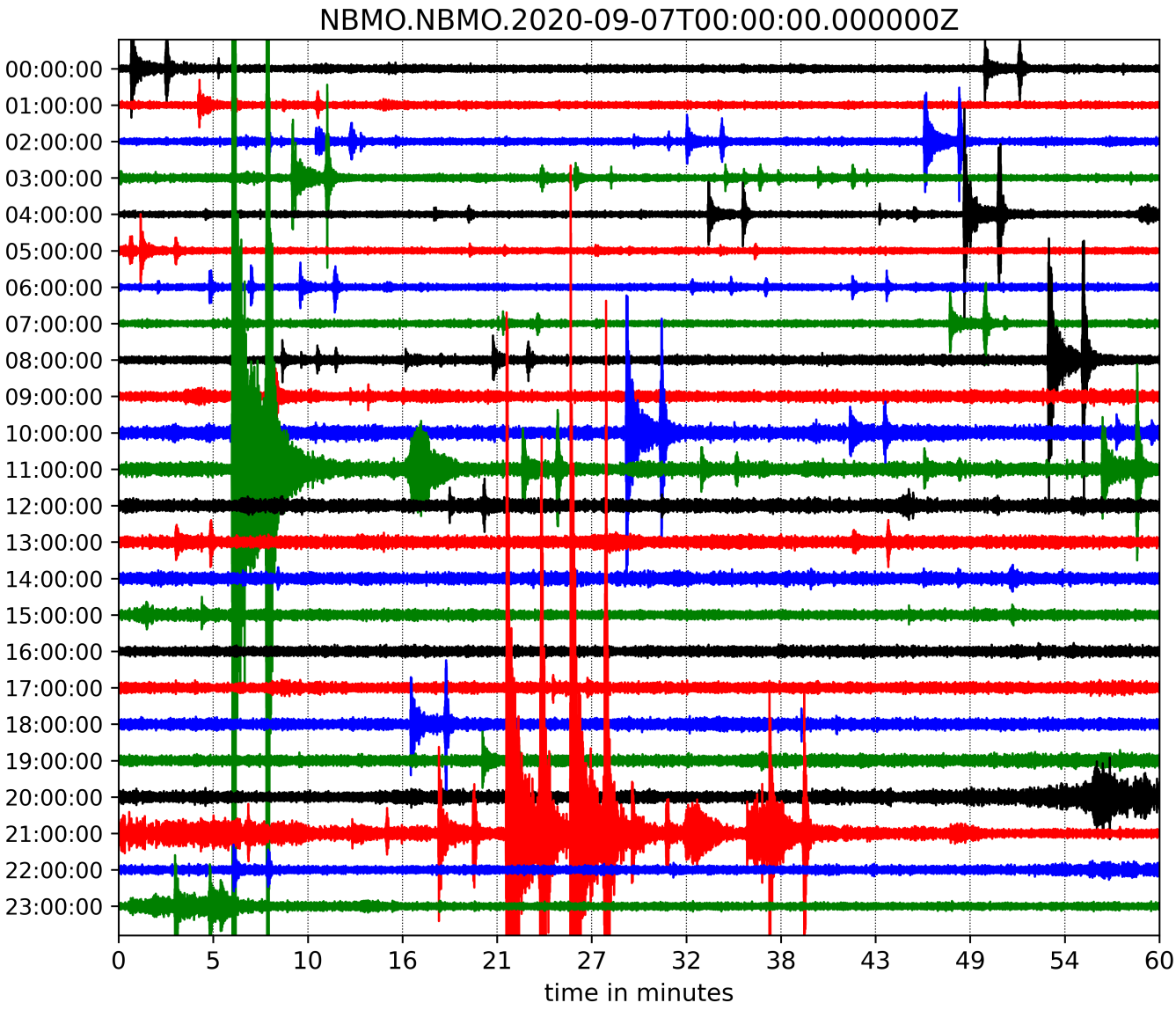

Figure 3: The 24 hour helicorder plot from the vertical component of NBMO seismic station for September 7, 2006. Horizontal colored lines present hour by hour interval time.

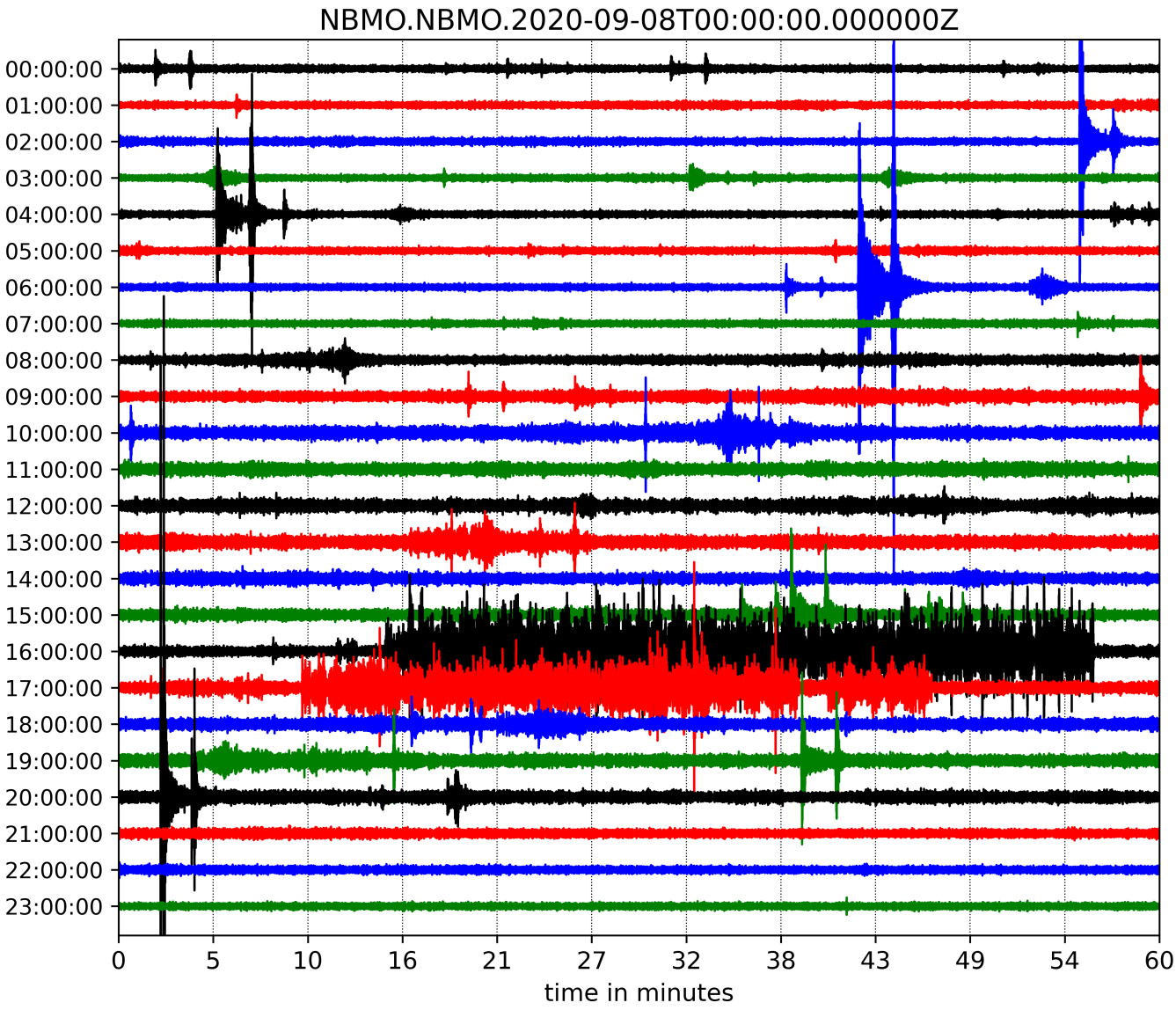

Figure 4: The 24 hour helicorder plot from the vertical component of NBMO seismic station for September 8, 2006. Horizontal colored lines present hour by hour interval time.

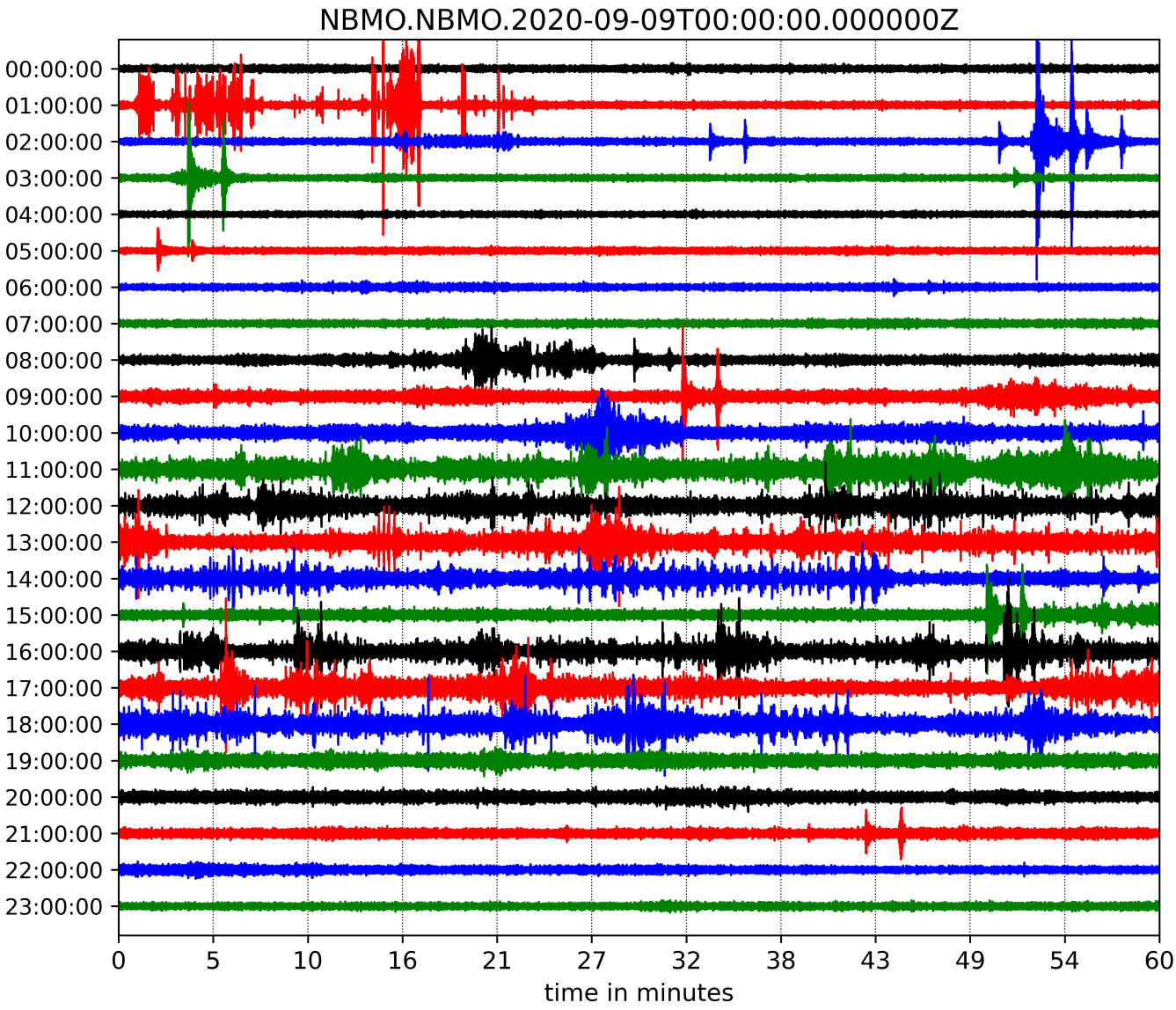

Figure 5: The 24 hour helicorder plot from the vertical component of NBMO seismic station for September 9, 2006. Horizontal colored lines present hour by hour interval time.

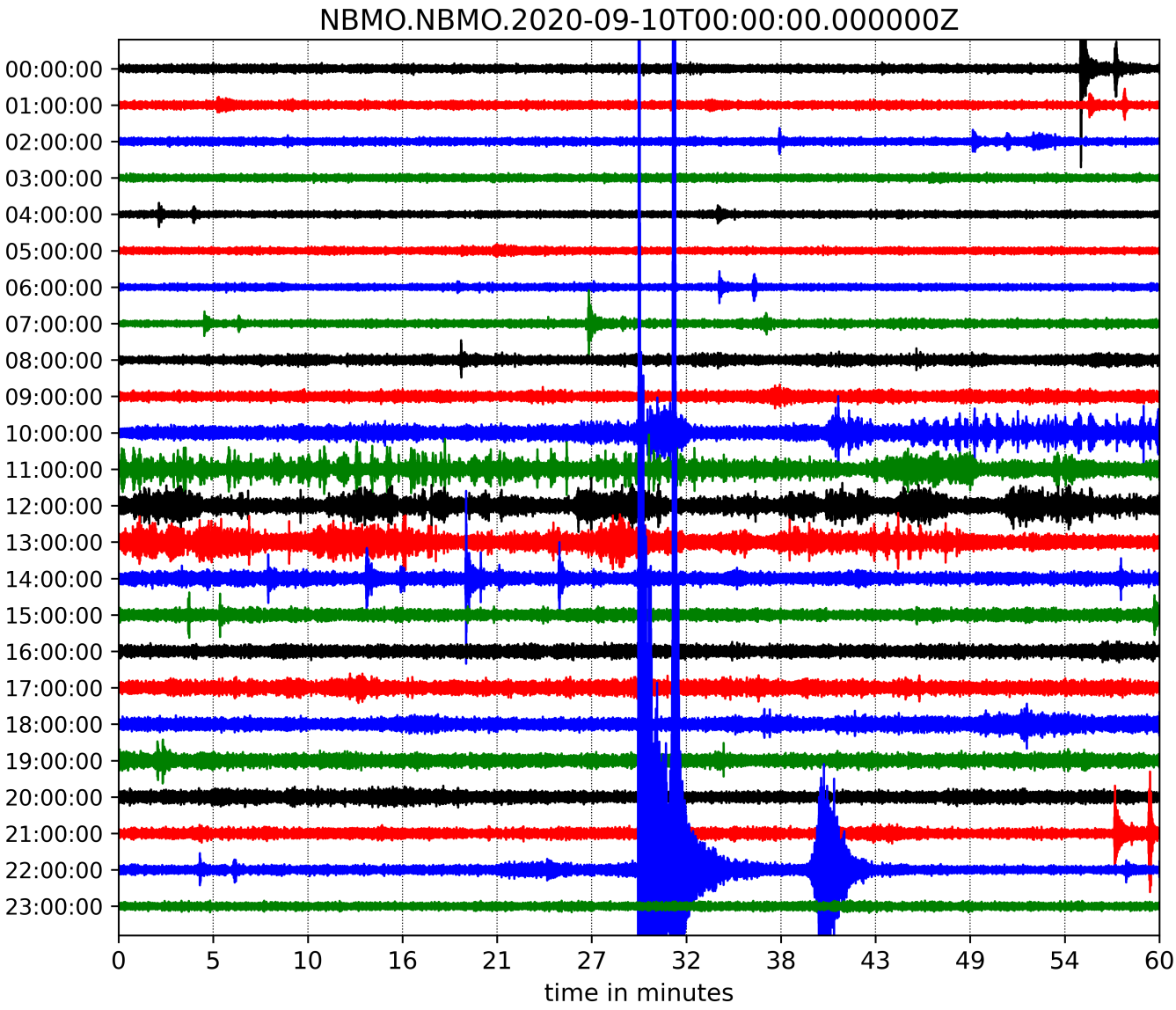

Figure 6: The 24 hour helicorder plot from the vertical component of NBMO seismic station for September 10, 2006. Horizontal colored lines present hour by hour interval time.

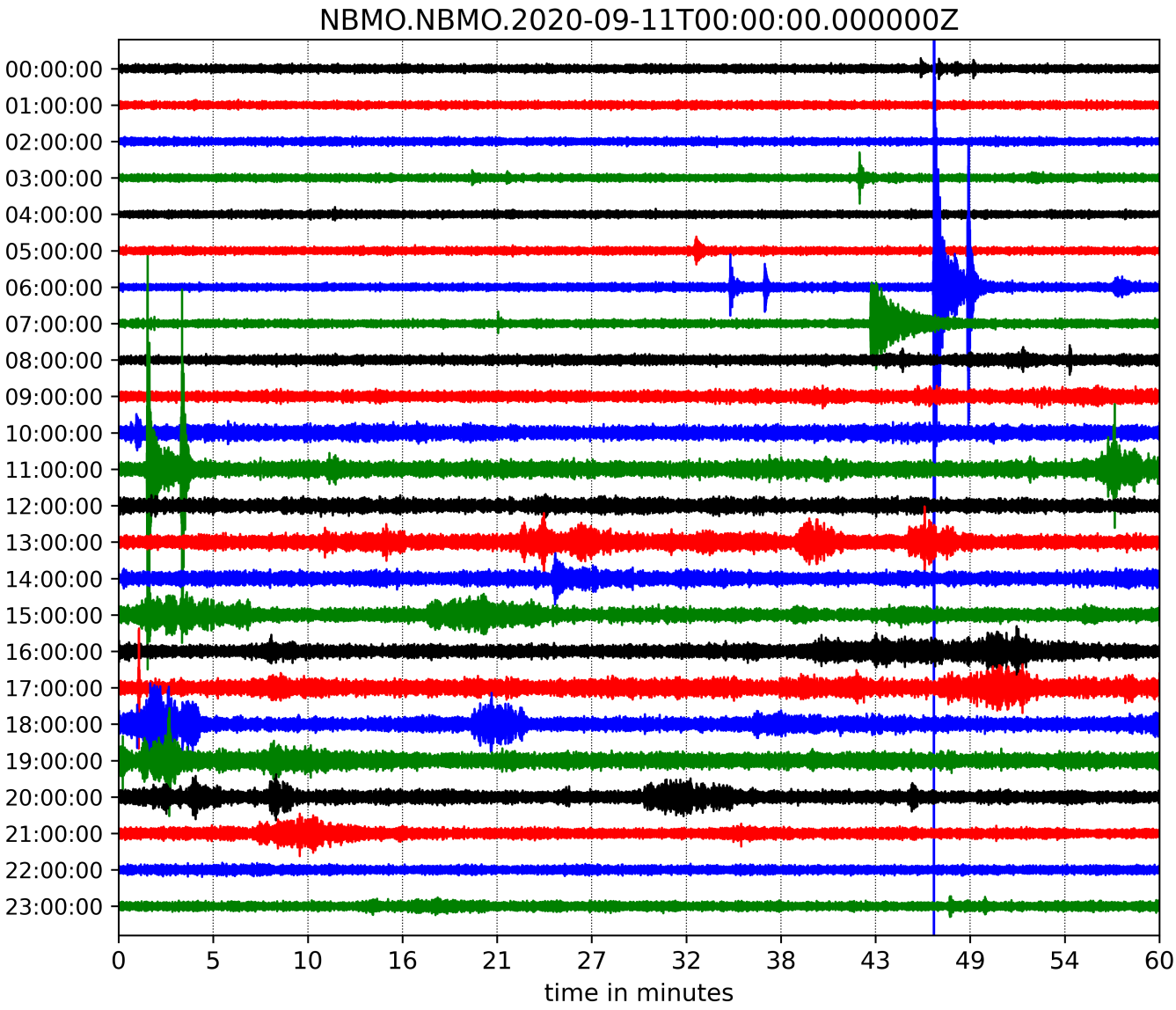

Figure 7: The 24 hour helicorder plot from the vertical component of NBMO seismic station for September 11, 2006. Horizontal colored lines present hour by hour interval time.

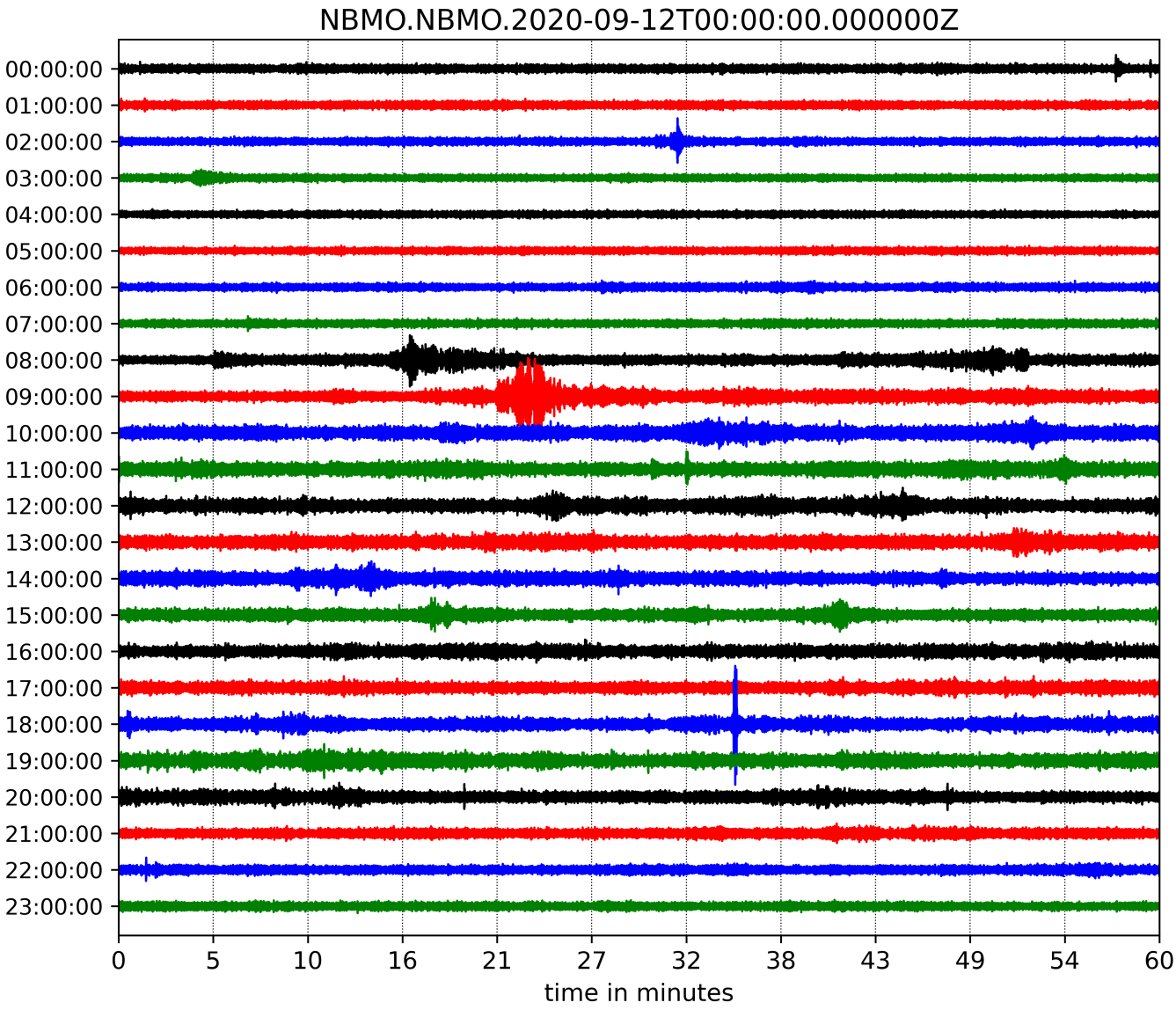

Figure 8: The 24 hour helicorder plot from the vertical component of NBMO seismic station for September 12, 2006. Horizontal colored lines present hour by hour interval time.

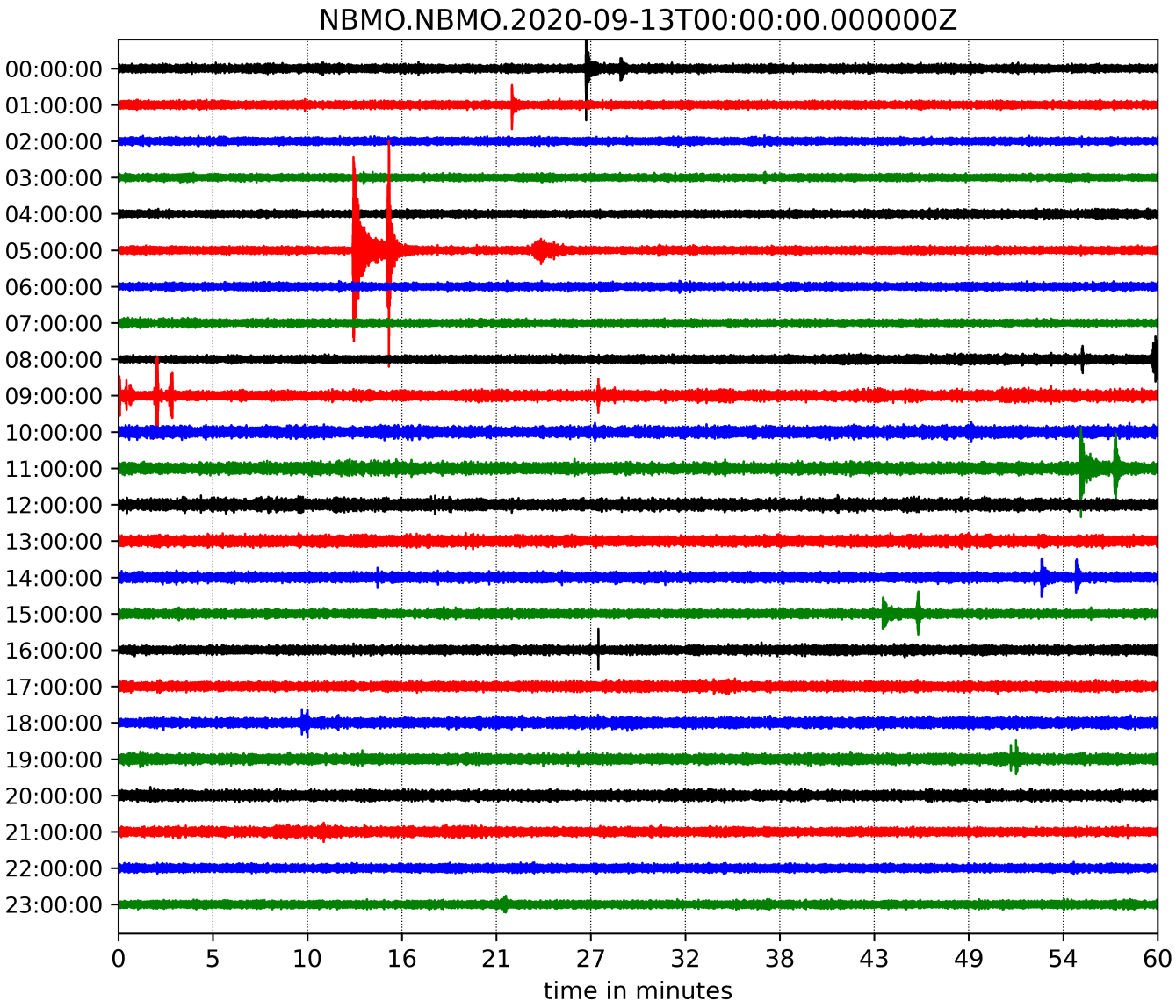

Figure 9: The 24 hour helicorder plot from the vertical component of NBMO seismic station for September 13, 2006. Horizontal colored lines present hour by hour interval time.

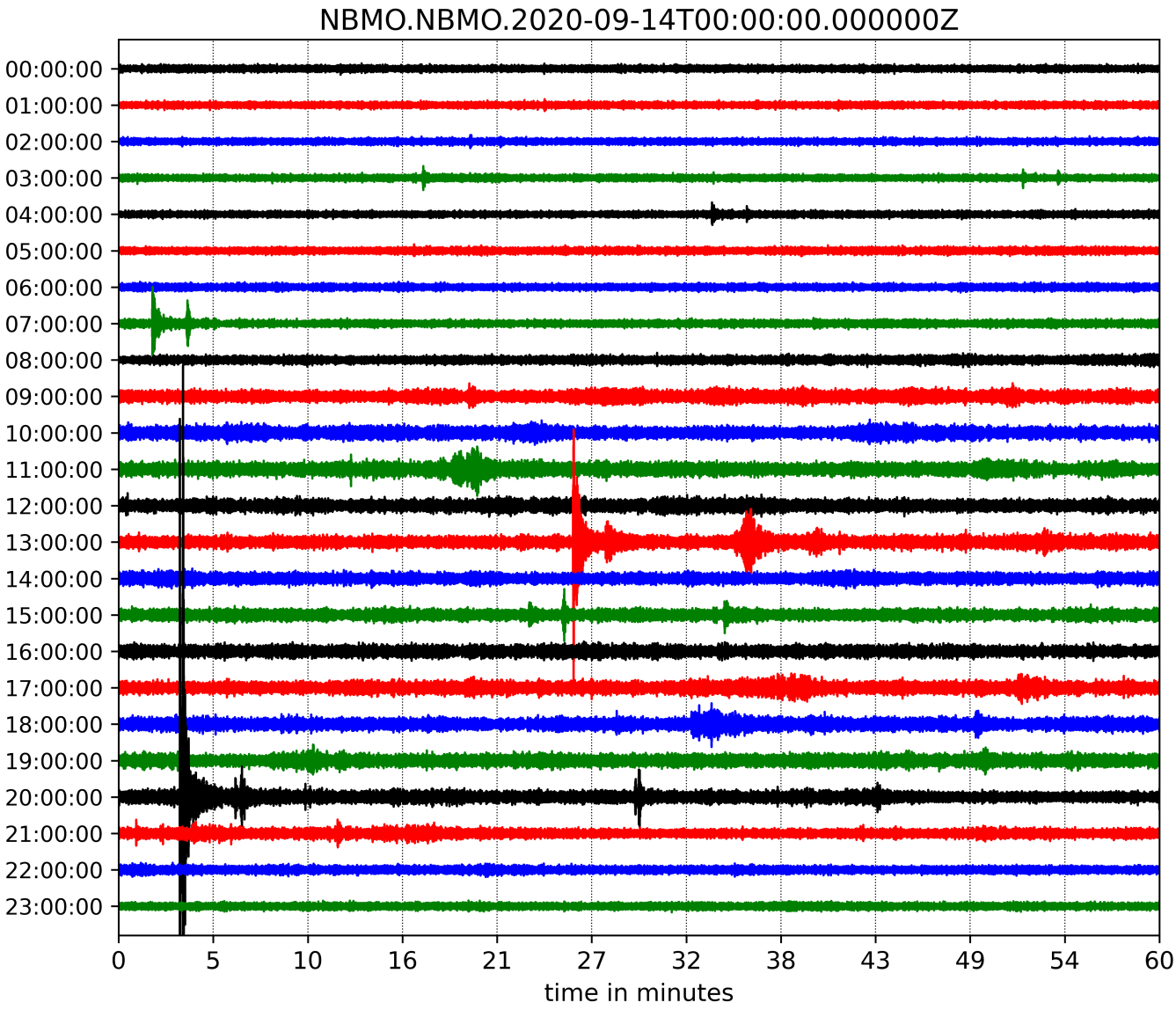

Figure 10: The 24 hour helicorder plot from the vertical component of NBMO seismic station for September 14, 2006. Horizontal colored lines present hour by hour interval time.

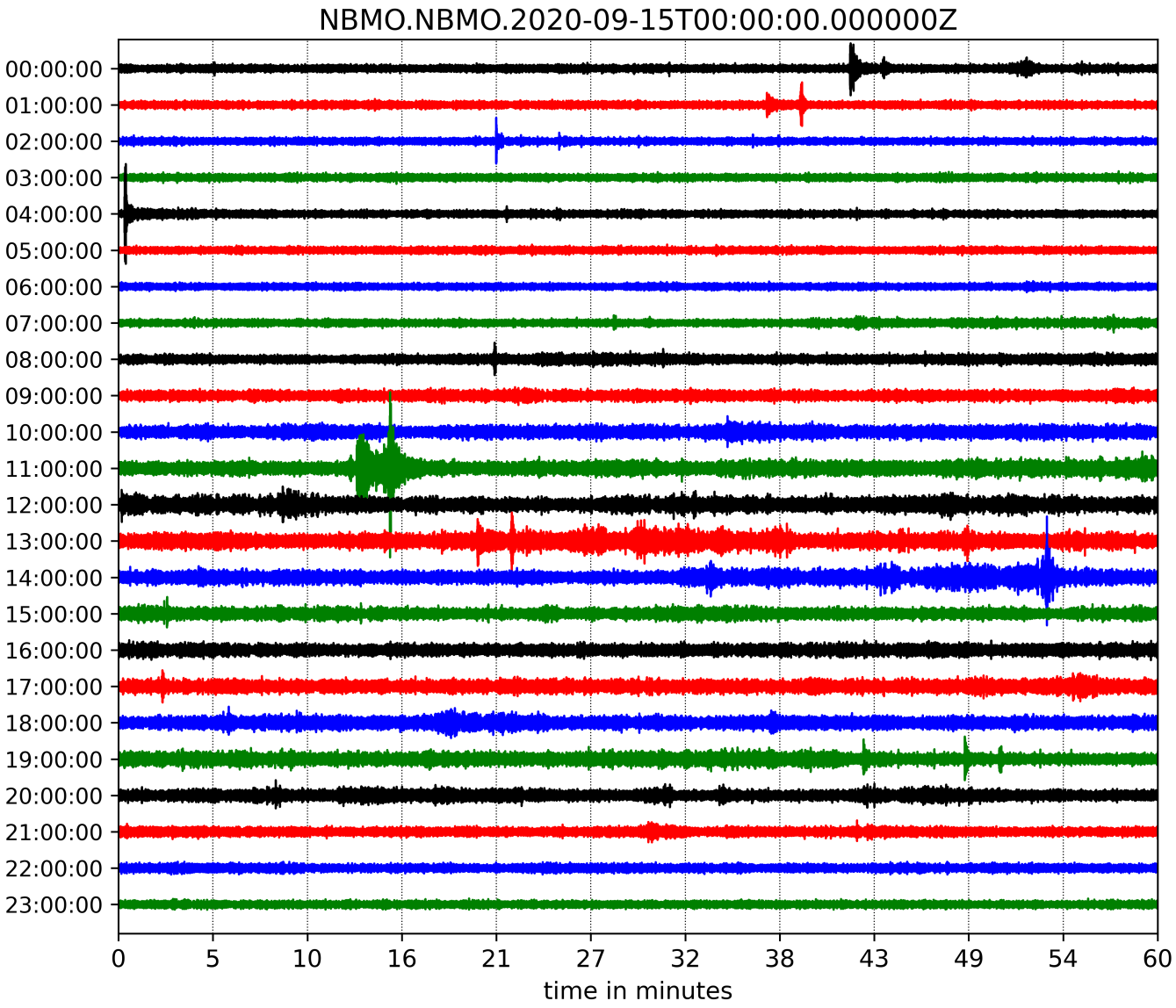

Figure 11: The 24 hour helicorder plot from the vertical component of NBMO seismic station for September 15, 2006. Horizontal colored lines present hour by hour interval time.

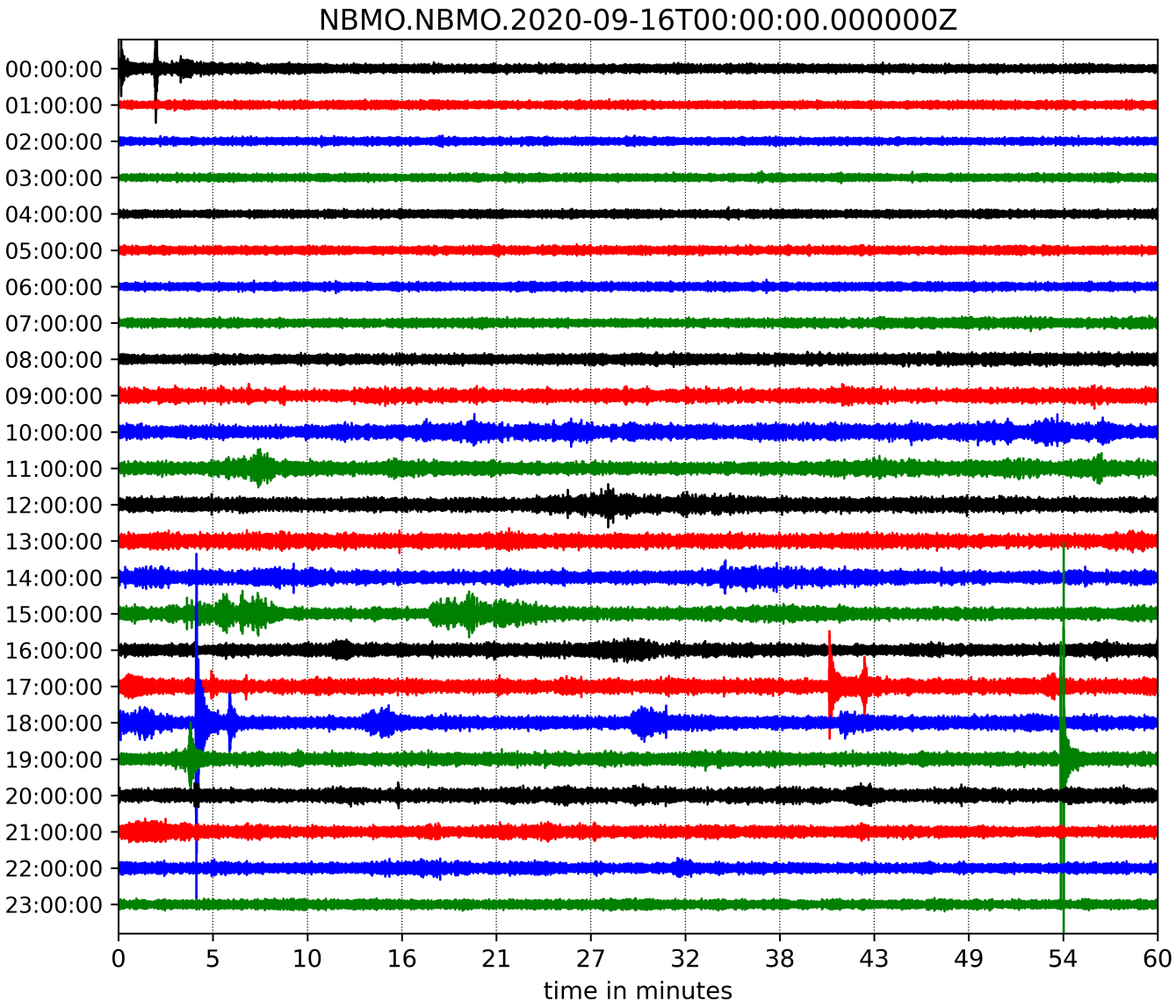

Figure 12: The 24 hour helicorder plot from the vertical component of NBMO seismic station for September 16, 2006. Horizontal colored lines present hour by hour interval time.

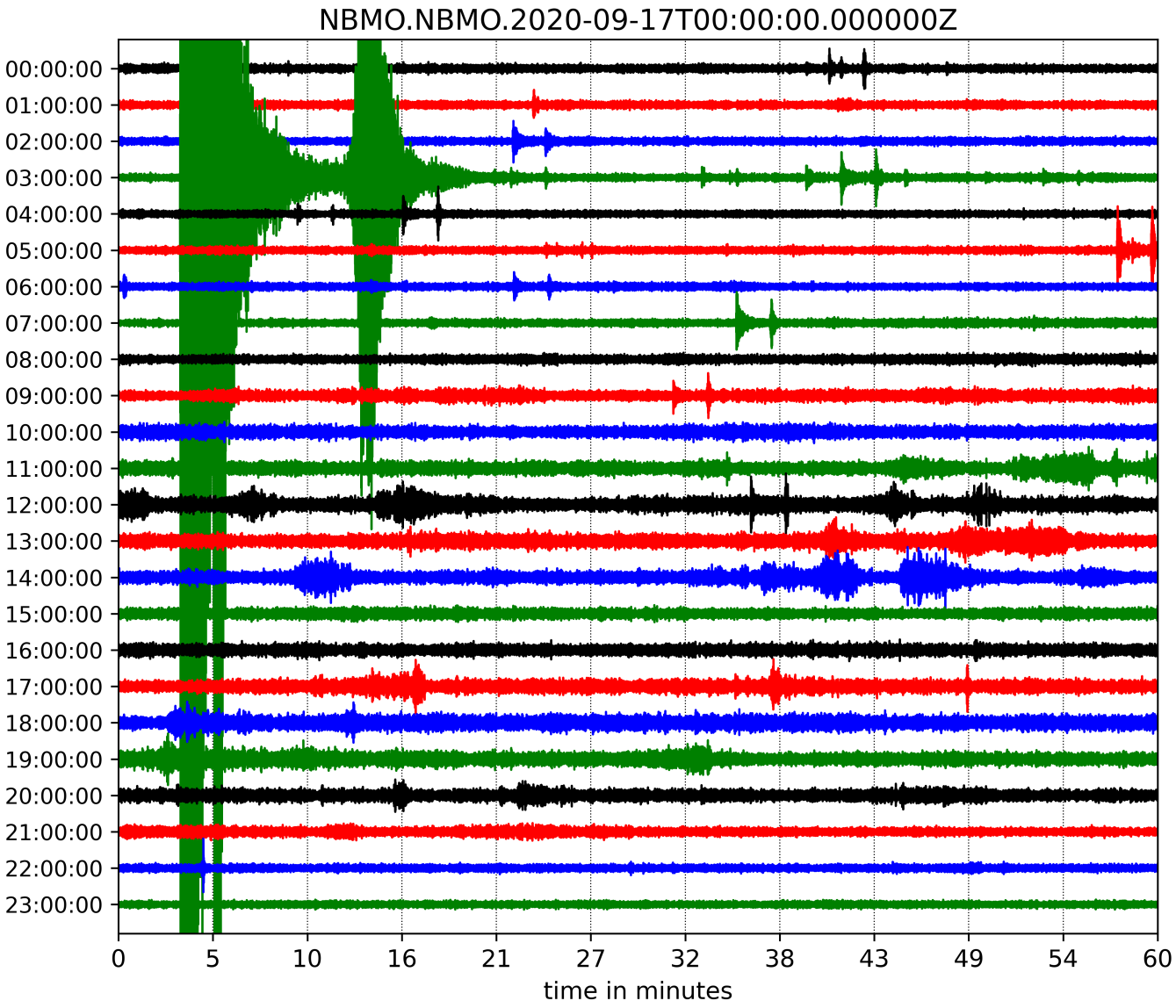

Figure 13: The 24 hour helicorder plot from the vertical component of NBMO seismic station for September 17, 2006. Horizontal colored lines present hour by hour interval time.

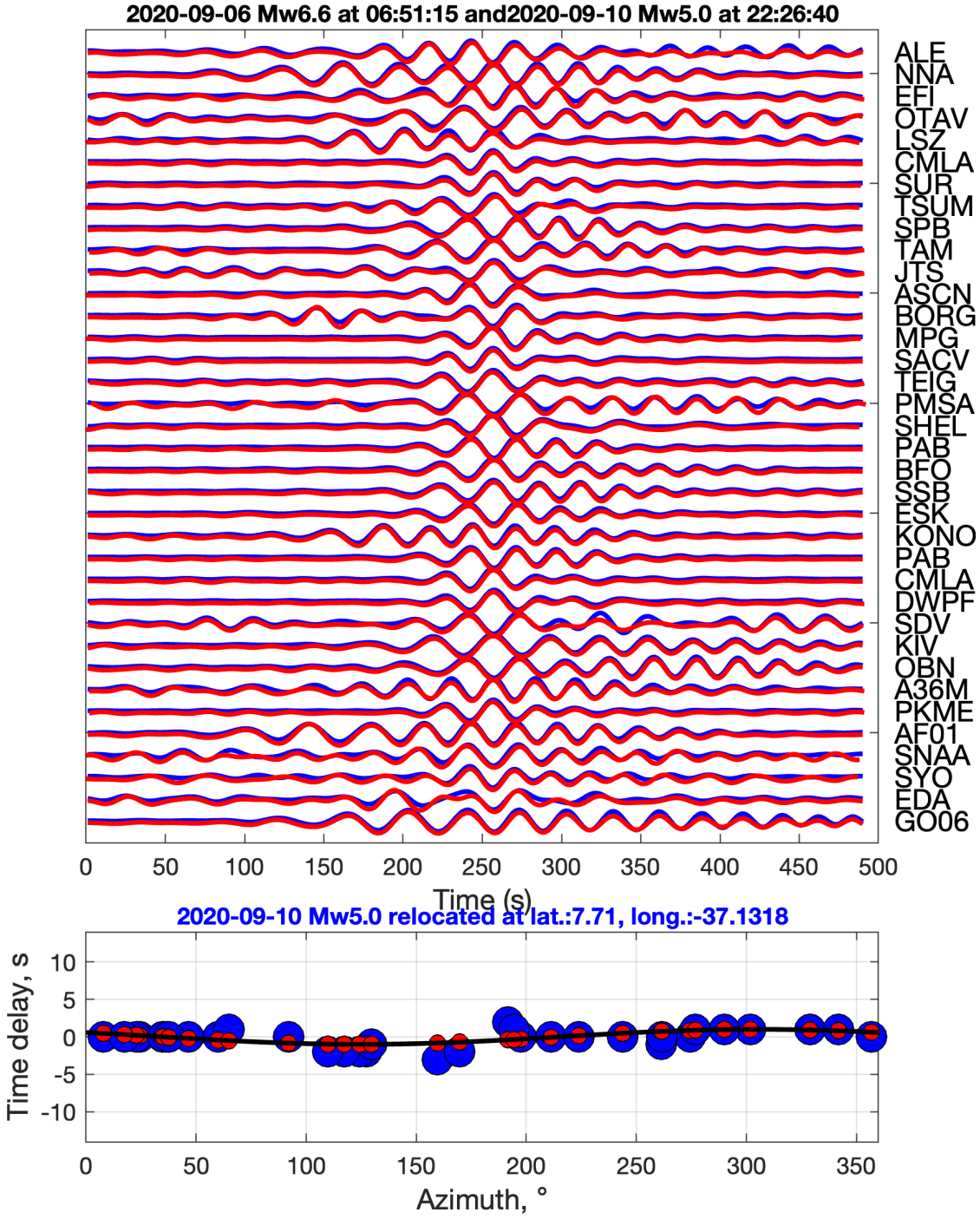

Figure 14: Relative relocation waveform fitting. Waveforms from the mainshock Mw 6.6 (shown in blue) are cross-correlated with seismograms from the time of the Sept. 10 at 22:26, Mw 5.0 (shown in red). The relative location is defined using the differential arrival times (bottom panel, blue circles), which are fitted using a grid search to minimize the L1 norm (black line and red dots). In this case, the location of the Mw 5.0 event was 3.8+/-1.7 km from the mainshock.

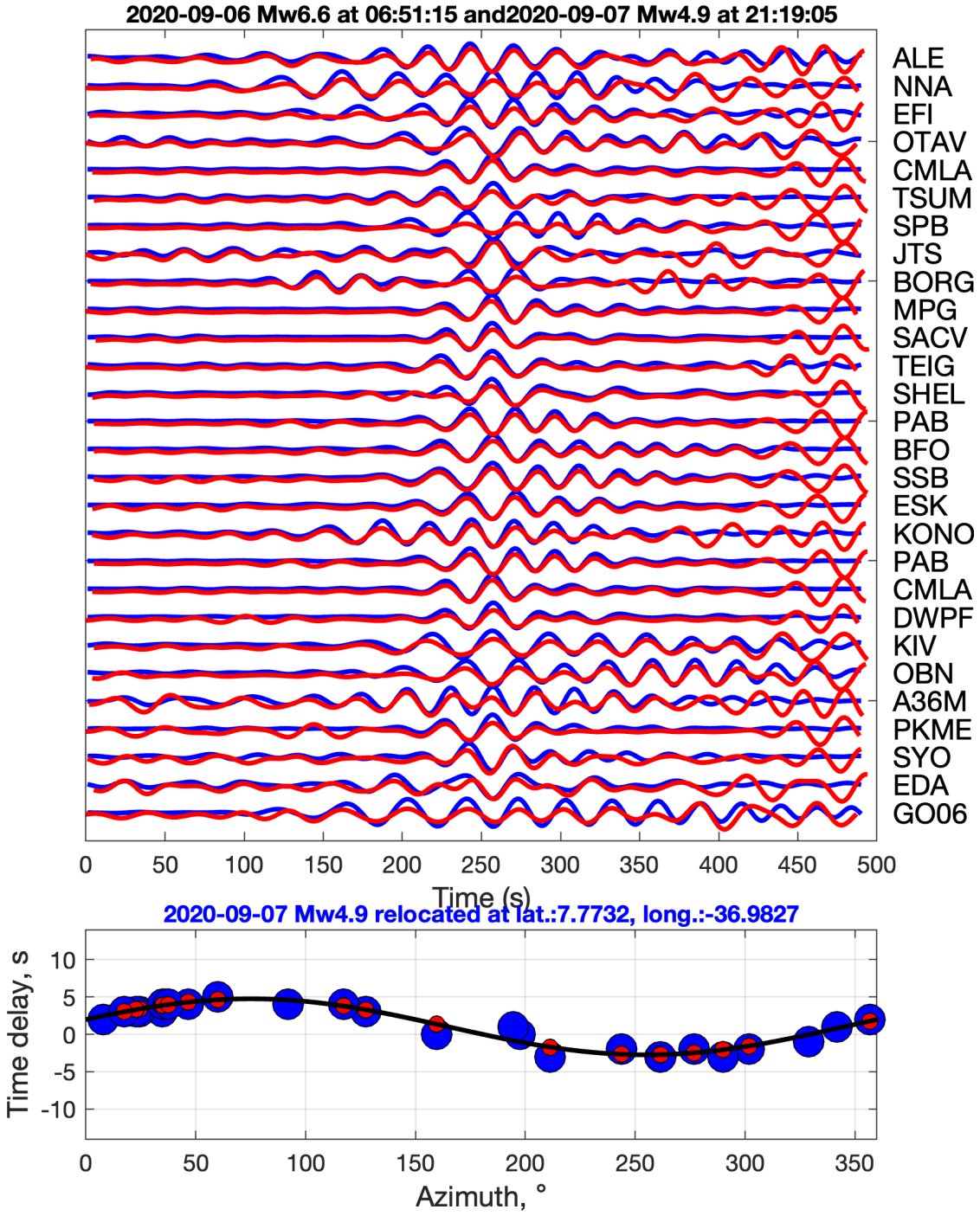

Figure 15: Relative relocation waveform fitting. Waveforms from the mainshock Mw 6.6 (shown in blue) are cross-correlated with seismograms from the time of the Sept. 7 at 21:19, Mw 4.9 (shown in red). The relative location is defined using the differential arrival times (bottom panel, blue circles), which are fitted using a grid search to minimize the L1 norm (black line and red dots). In this case, the location of the Mw 4.9 event was 14.2+/-1.5 km from the mainshock.

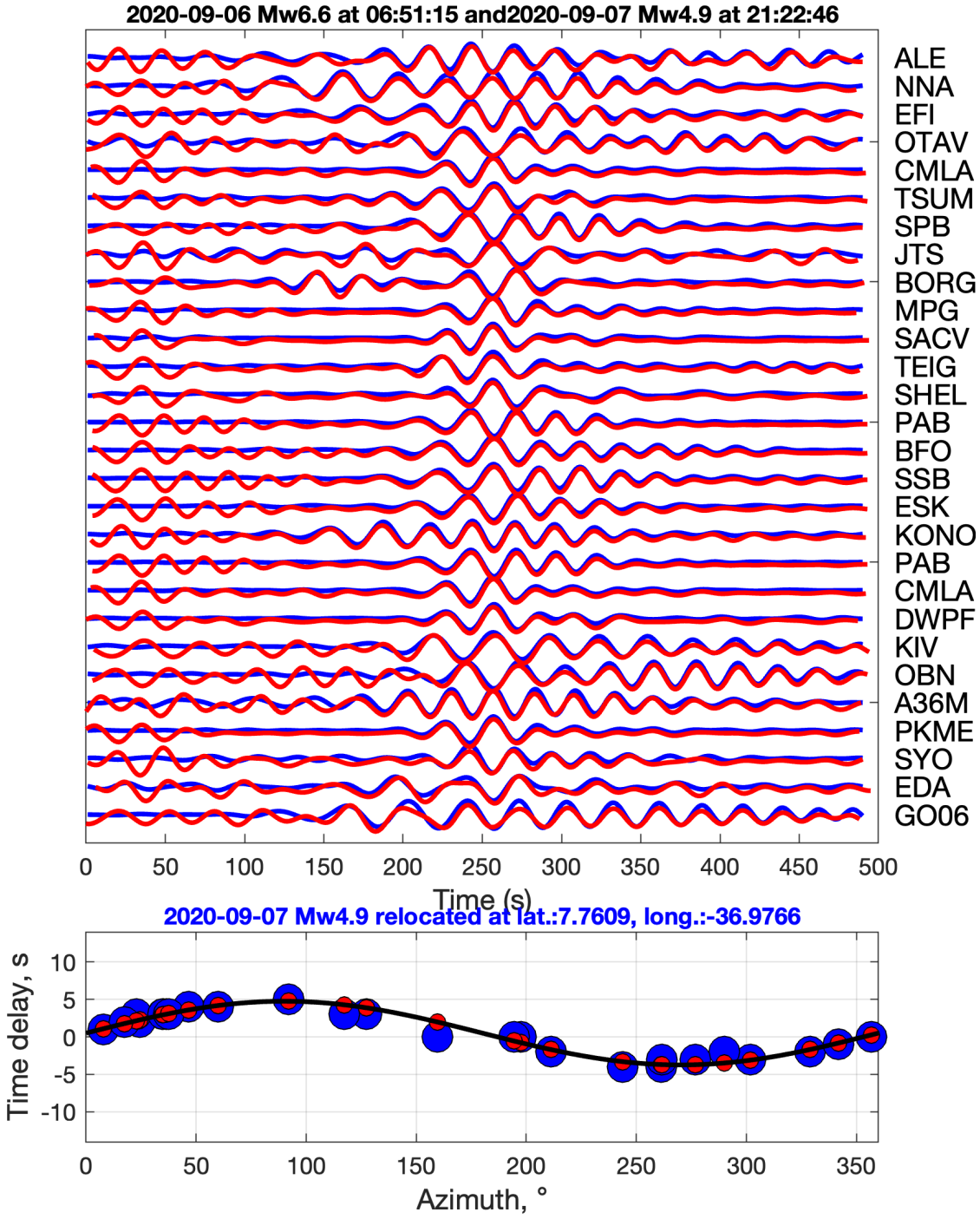

Figure 16: Relative relocation waveform fitting. Waveforms from the mainshock Mw 6.6 (shown in blue) are cross-correlated with seismograms from the time of the Sept. 7 at 21:22 Mw 4.9 (shown in red). The relative location is defined using the differential arrival times (bottom panel, blue circles), which are fitted using a grid search to minimize the L1 norm (black line and red dots). In this case, the location of the Mw 4.9 event was 14.5+/-1.5 km from the mainshock.

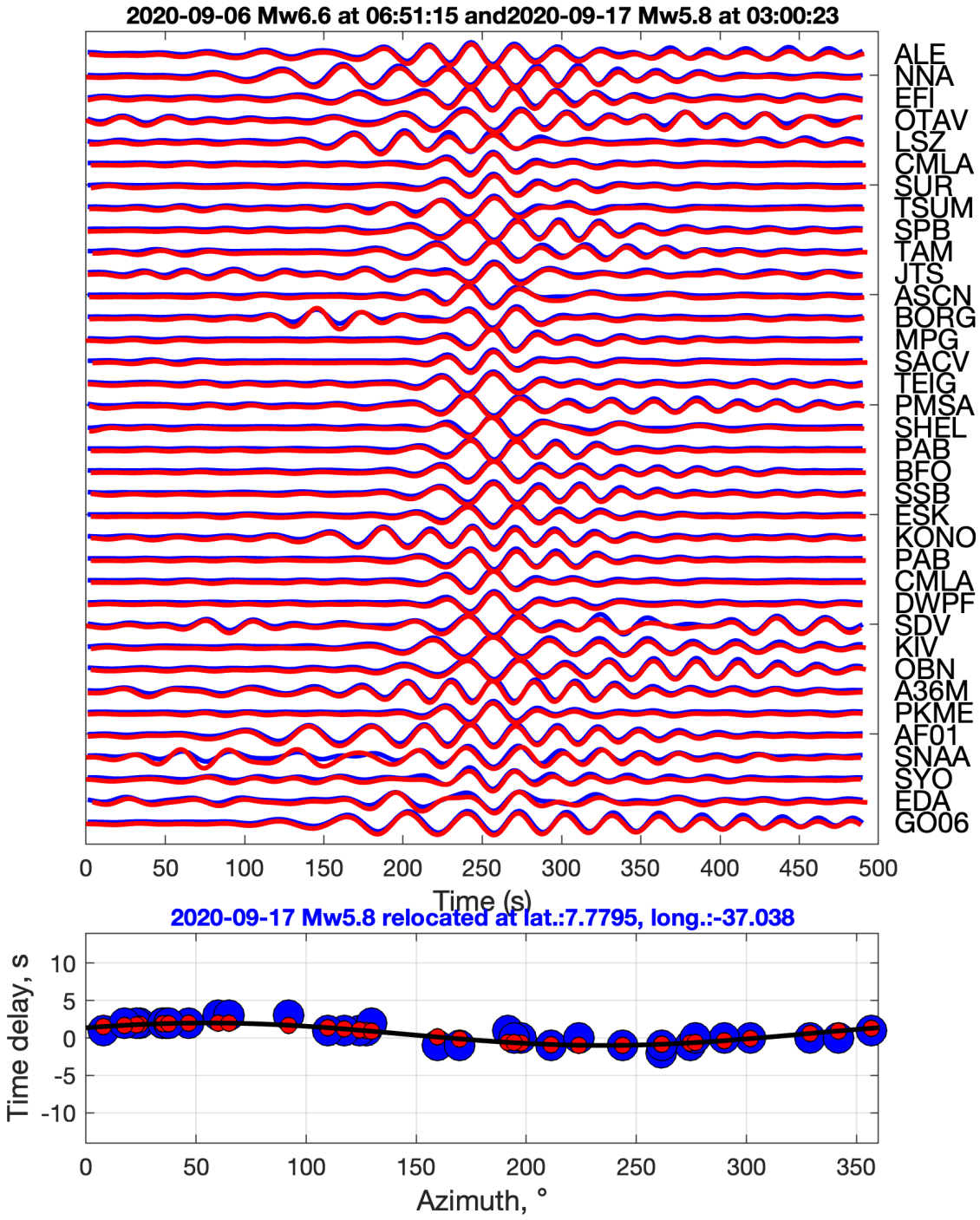

Figure 17: Relative relocation waveform fitting. Waveforms from the mainshock Mw 6.6 (shown in blue) are cross-correlated with seismograms from the time of the Sept. 17 at 03:00, Mw 5.8 (shown in red). The relative location is defined using the differential arrival times (bottom panel, blue circles), which is fitted using a grid search to minimize the L1 norm (black line and red dots). In this case, the location of the Mw 5.8 event was 8.3+/-1.2 km from the mainshock.

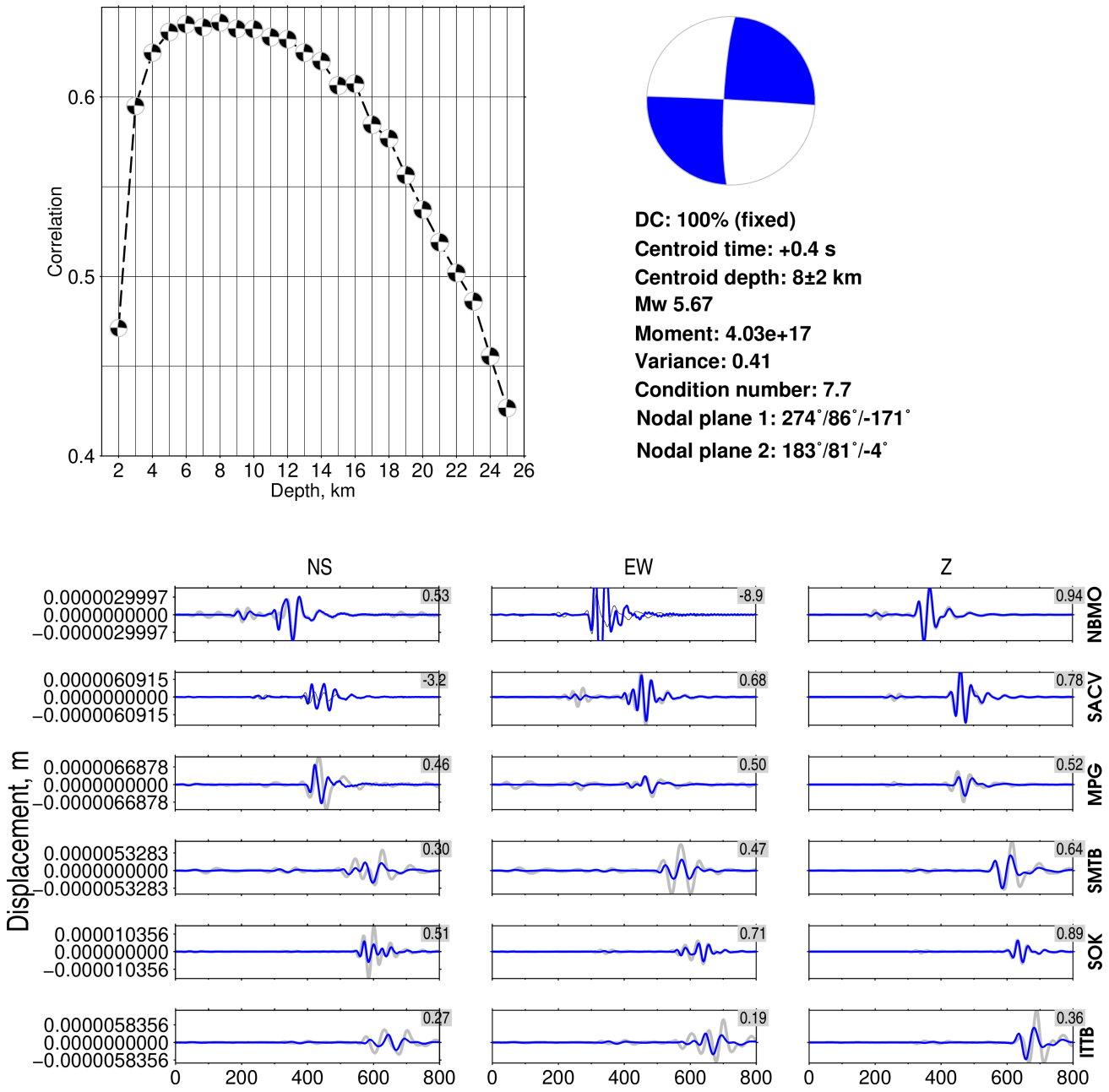

Figure 18: Real/synthetic waveform fitting of the focal depth analysis to the aftershock Mw 5.8. Gray/blue waveforms refer to the real/modeled obtained with the best-fitting source position at 8 km focal depth.

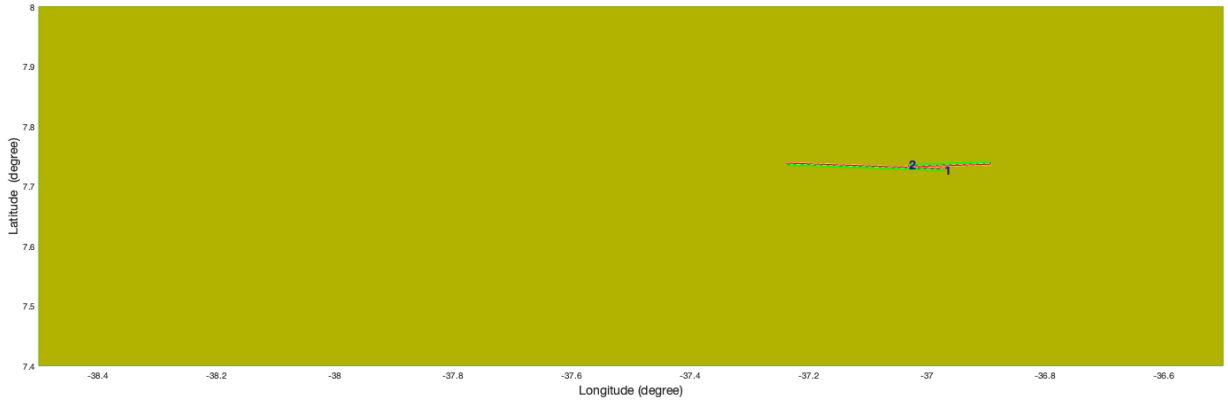

Figure 19: 2D view of the rupture coordinates plane applied in Coulomb modeling using the Coulomb3 package. Trace 1 refers to the 2008 Mw 5.6. Trace 2/3 indicated the 2020 Mw 6.6 and 2020 Mw 5.8.

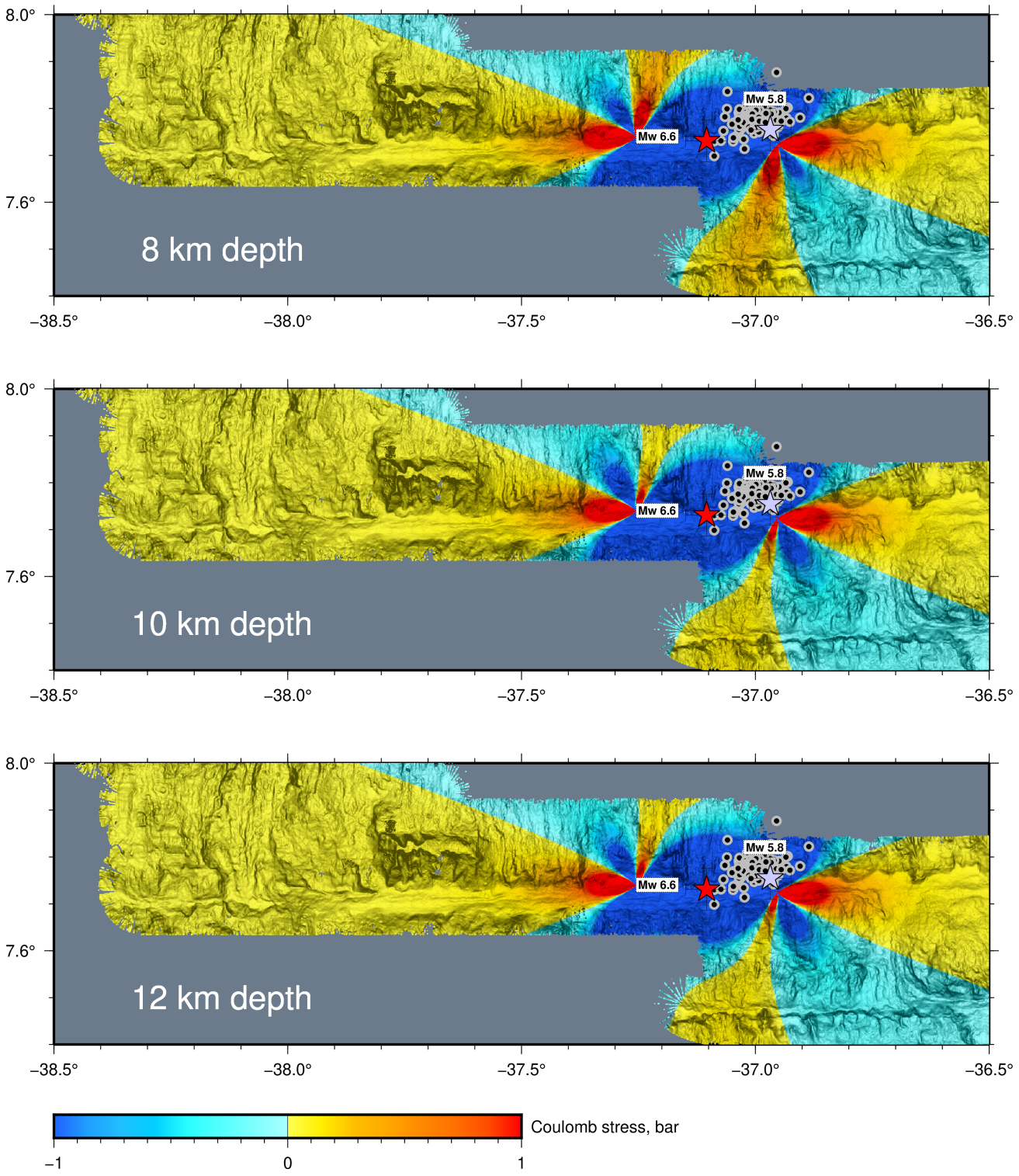

Figure 20: Coulomb stress change of the mainshock Mw 6.6 modeled using the Coulomb3 package with 8, 10, and 12 km vertical faulting range.

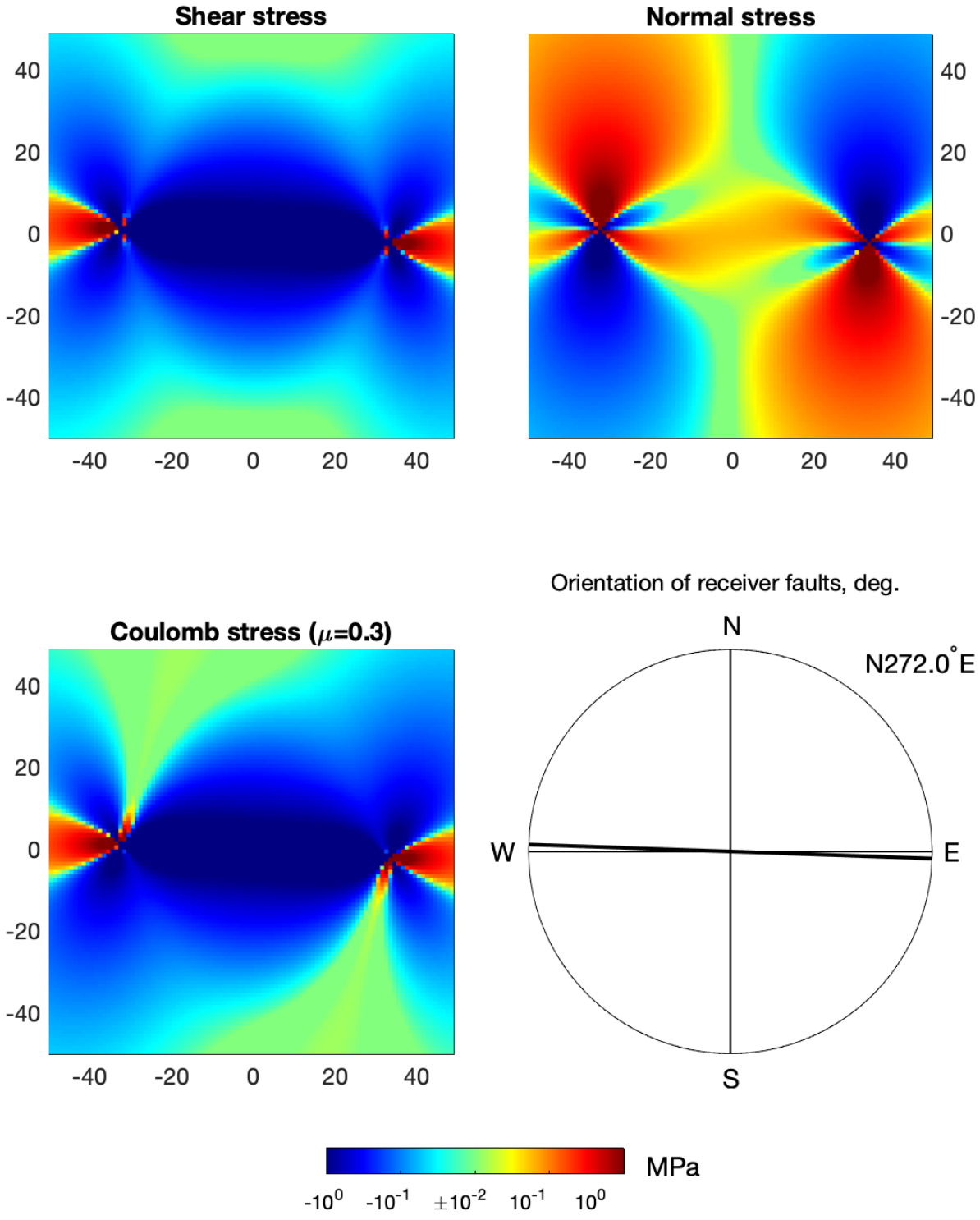

Figure 21: Coulomb stress change of the mainshock Mw 6.6 modeled using the DIS3D code using a friction rate of 0.3.